

Supplementary Information

Investigating the effect of a fluoroethylene carbonate additive on lithium deposition and the solid electrolyte interphase in lithium metal batteries using *in situ* NMR spectroscopy

Anna B. Gunnarsdóttir,¹ Sundeep Vema,^{1,2} Svetlana Menkin,¹ Lauren E. Marbella,^{1,3}
and Clare P. Grey^{1*}

1. Department of Chemistry, University of Cambridge, Lensfield Road, Cambridge, CB2 1EW, U.K
2. The Faraday Institution, Quad One, Harwell Science and Innovation Campus, Didcot OX11 0RA, U.K
3. Present address: Department of Chemical Engineering, Columbia University, 500 W 120th St, New York, NY 10027, USA

*Corresponding author: Professor Clare P. Grey, email: cpg27@cam.ac.uk

Table of Contents

1. Methodology to quantify the NMR signal of Li metal	2
2. Deconvolution of the ⁷ Li metal intensity measured with <i>in situ</i> NMR.....	3
3. Symmetrical Li coin cells – Galvanostatic cycling.....	4
4. Gradient slope of mass change measured with <i>in situ</i> NMR.....	5
5. Pulse plating.....	5
6. SEM figures	6
7. The effect of pitting on the NMR measurements.....	8
8. Isotope exchange measurements.....	9
9. Numerical model of isotope exchange – Additional figures	10
10. Impedance spectroscopy	12
11. <i>In situ</i> NMR spectra and the electrochemistry.....	14
References.....	16

1. Methodology to quantify the NMR signal of Li metal

The theory used to quantify the amount of deposited microstructures is based on previous work by Bhattacharyya *et al.* and Chandrashekar *et al.*^{1,2} For an radiofrequency (rf) field of strength ω_1 , the field inside the metal at depth x from the metal surface is given by

$$\omega_1(x) = \omega_1(0)e^{-\frac{x}{d}} \quad (\text{Eq. S1})$$

where d is the skin depth³:

$$d = \sqrt{\frac{\rho}{\pi\mu_0\mu_r\nu}} = 12.1 \mu\text{m} \quad (\text{Eq. S2})$$

and ρ the resistivity of the metal (94.7 n Ω for Li metal at 298 K), μ_0 is the permeability of the vacuum ($4\pi \cdot 10^{-7}$ m kg/ s²A²), μ_r is the relative permeability of the medium ($\mu_r = 1.4$ for Li metal) and ν is the frequency of the applied rf field (116.7 MHz in this study).⁴ We see from equation S1 that the rf field varies as a function of distance and thus the flip angle experienced by the Li spins in the bulk Li metal is not constant.^{1,2,5}

For direct excitation in NMR, the signal intensity S depends on the ω_1 strength of the applied rf and τ_p , the duration of the rf pulse. Following the approach of Chandrashekar *et al.*² and making use of the reciprocity principle,⁶ the signal intensity, S , obtained from the total surface area A of a metal sample is:

$$S = \frac{A s_0}{\omega_1(0)} \int_0^\infty dx [\omega_1(x) \sin(\omega_1(x)\tau_p)] \quad (\text{Eq. S3})$$

where s_0 is the signal intensity per unit volume. Plugging in equation S1 gives:

$$S = \frac{A s_0}{\omega_1(0)} \int_0^\infty dx [\omega_1(x) \sin(\omega_1(x)\tau_p)] = \frac{A s_0 d}{\omega_1(0)\tau_p} (1 - \cos(\omega_1\tau_p)) \quad (\text{Eq. S4})$$

From equation S4, the maximum signal obtained for a pristine Li metal electrode corresponds to a flip angle of $\omega_1(0)\tau_p \approx 2.32 \text{ rad} \approx 133^\circ$.

After electrodeposition, the signal arising from the Li deposits, assuming no skin depth effect of the microstructures is:² $S_{micro} = V_\mu s_0 \sin(\omega_1(0)\tau_p)$.

Thus, the total signal intensity as a function of time during Li metal deposition:

$$S(t) = S_{metal}(t) + S_{micro}(t) \quad (\text{Eq. S5})$$

And assuming no attenuation of the bulk metal signal, $S_{metal}(t) = S(0)$ and

$$S(t) = S(0) + S_{micro}(t) = S_0 + V_\mu s_0 \sin(\omega_1(0)\tau_p) \quad (\text{Eq. S6})$$

Solving for the volume of deposited microstructures: $V_\mu(t) = \frac{S(t)-S(0)}{s_0 \sin(\omega_1(0)\tau_p)}$ and multiplying by $S(0)/S(0)$ results in:

$$V_\mu(t) = \frac{\frac{A d}{\omega_1(0)\tau_p} (1 - \cos(\omega_1\tau_p))}{\sin(\omega_1(0)\tau_p)} \frac{S(t)-S(0)}{S(0)} \quad (\text{Eq. S7})$$

Which for a flip angle of 133° gives $V_\mu(t) = \frac{0.728 Ad}{0.732} \frac{S(t)-S(0)}{S(0)} = 0.995 Ad \frac{S(t)-S(0)}{S(0)}$

and for 90° , $V_\mu(t) = 0.636 Ad \frac{S(t)-S(0)}{S(0)}$.

Thus the change in signal intensity can be readily converted to the amount of microstructure deposited. The density of lithium at room temperature is 0.53 g/cm^3 , so the total mass of microstructures $m(t) = V_\mu(t) \frac{0.53g}{\text{cm}^3}$.

2. Deconvolution of the ^7Li metal intensity measured with *in situ* NMR

The deconvolution of the *in situ* NMR spectra was carried out in R, using a pseudo-Voigt curve and least-squares fitting with 3-4 peaks; two metal peaks (Metal 1 and Metal 2), referred to as „bulk metal“ in the paper and two microstructural peaks (Micro 1 and Micro 2). Adding a second peak to fit the bulk metal is consistent with earlier work, the asymmetry of the peak assigned to the edges of the metal electrodes and inhomogeneities on the metal surface such as pitting.^{5,7,8} Adding a second microstructures peak (Micro 2) was only needed when using 2 mA/cm^2 in LP30 electrolyte and is assigned to microstructures growing relatively further away from the electrode's surface. The fitting parameters used are the height, position, width (half width half maximum, HWHM) and a ratio of the Gaussian/Lorentzian lineshape. Constraints were added to the chemical shift of the peaks, Metal 1: 245-247.5 ppm, Metal: 247.5- 252.5 ppm, Micro 1: 257.5-262.5 ppm and Micro 2: 267.5 – 272.5 ppm.

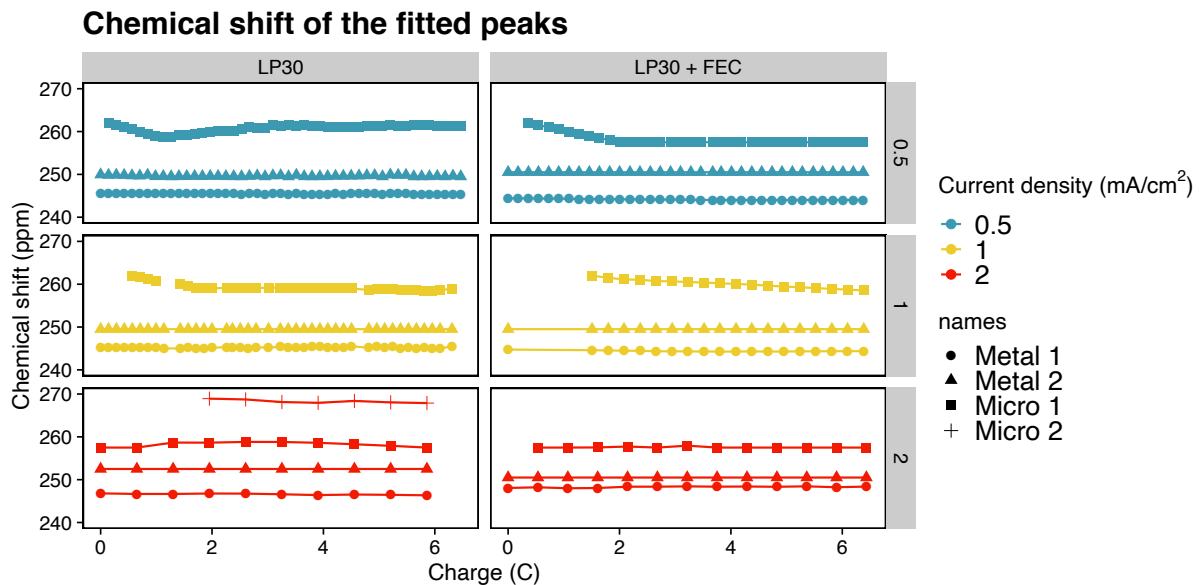


Figure S1. The chemical shift of the fitted peaks at different current densities in the two electrolyte systems LP30 (left) and LP30 + FEC (right).

3. Symmetrical Li coin cells – Galvanostatic cycling

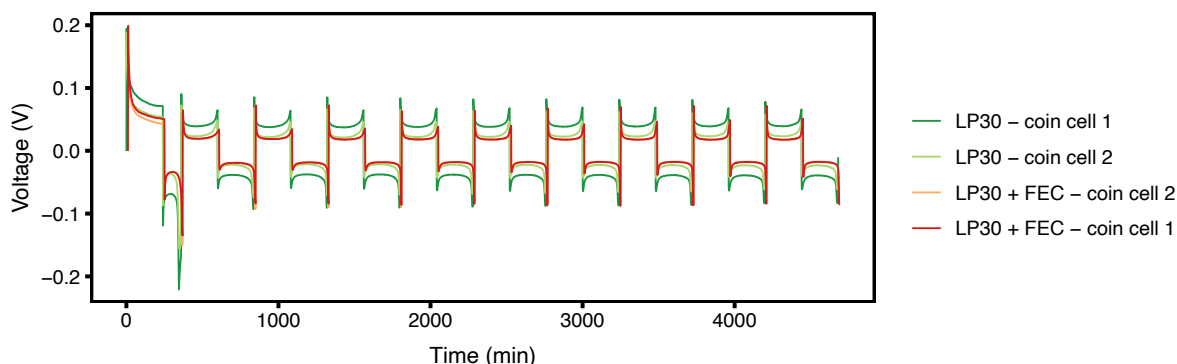


Figure S2. Constant plating $0.5 \text{ mA/cm}^2 - 2 \text{ mAh/cm}^2 - 10$ cycles. Pitting occurs earlier in LP30 electrolyte (green) compared to LP30 + 10% FEC (orange) indicating either earlier onset of pitting and formation of dead Li or less microstructures formed on the surface. Figure 4a in the main text shows the galvanostatic cycling for ‘coin cell 1’ in this figure.

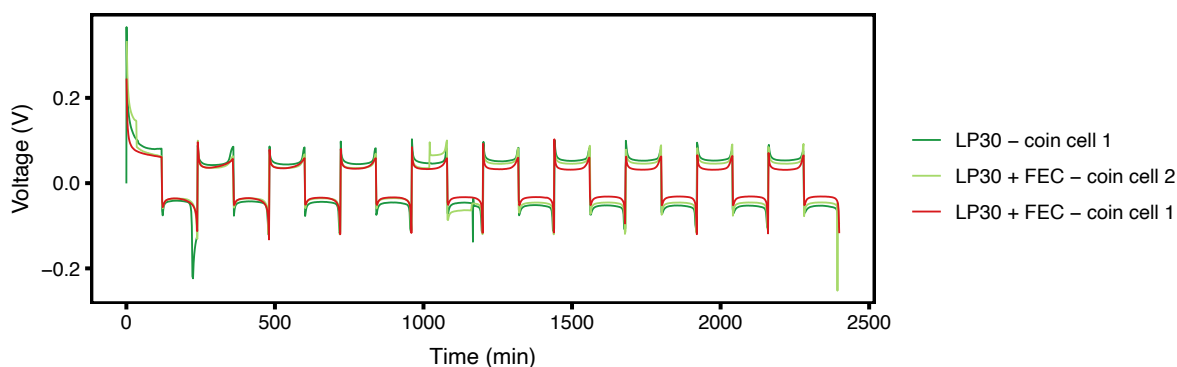


Figure S3. Constant plating $1 \text{ mA/cm}^2 - 2 \text{ mAh/cm}^2 - 10$ cycles. Pitting occurs earlier in LP30 electrolyte (green) compared to LP30 + 10% FEC (orange) indicating either earlier onset of pitting and formation of dead Li or less microstructures formed on the surface.

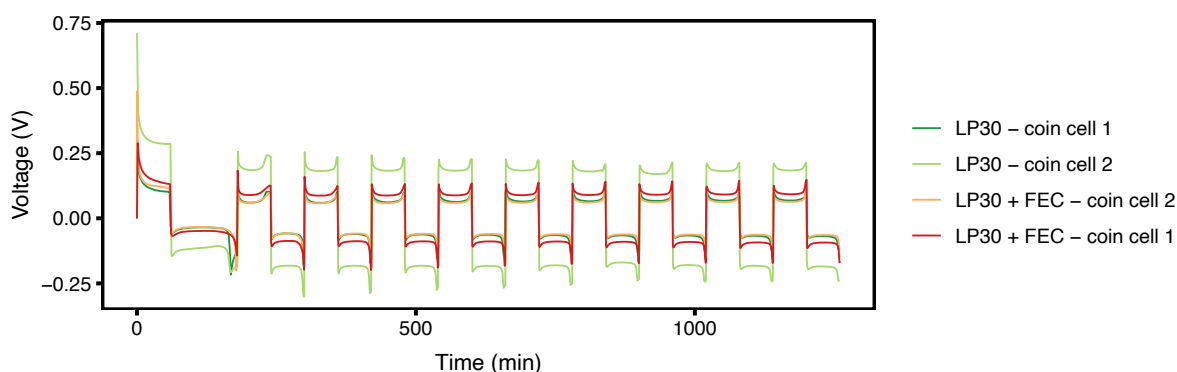


Figure S4. Constant plating $2 \text{ mA/cm}^2 - 2 \text{ mAh/cm}^2 - 10$ cycles. Pitting occurs earlier in LP30 electrolyte (green) compared to LP30 + 10% FEC (orange) indicating either earlier onset of pitting and formation of dead Li or less microstructures formed on the surface.

4. Gradient slope of mass change measured with *in situ* NMR

Table S1. Gradient slope of the linear fit of the mass change vs. charge for the deconvoluted peaks in LP30 and LP30 + FEC electrolytes and constant current plating.

0.5 mA/cm²	LP30 [mg/C]	LP30 + 10% FEC [mg/C]
Microstructural peak	0.053	0.082
Metal peak	-0.031	-0.029
Whole intensity	0.023	0.053
1 mA/cm²	LP30 [mg/C]	LP30 + 10% FEC [mg/C]
Microstructural peak	0.02	0.08
Metal peak	0.01	-0.02
Whole intensity	0.03	0.07
2 mA/cm²	LP30 [mg/C]	LP30 + 10% FEC [mg/C]
Microstructural peak	0.062	0.048
Metal Peak	0.027	0.040
Whole intensity	0.087	0.087
Electrochemistry	0.072	0.072

Table S2. Gradient slope of the linear fit to the microstructural mass increase vs. charge for pulse plating (PP) in LP30 electrolyte with current density 1 mA/cm² and various pulse lengths, T_{ON}, T_{OFF} presented in Figure S9.

Pulse method	Gradient slope [mg/C]
Constant plating 0.5 mA/cm ²	0.053
PP, 1s:1s	0.084
PP, 500ms:500ms	0.073
PP, 50ms:50ms	0.079
PP, 5ms:5ms	0.081
Electrochemistry	0.072

5. Pulse plating

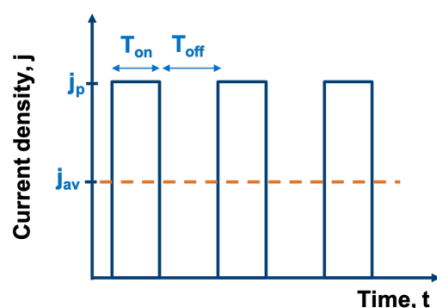


Figure S5. Schematic of the pulse plating showing the pulse lengths, T_{ON} and T_{OFF}.

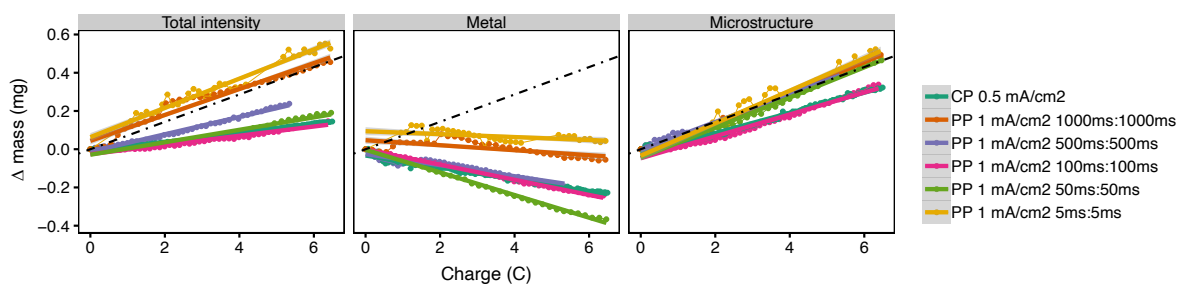


Figure S6. The deconvoluted intensities of the *in situ* NMR spectra during constant plating and pulse plating (PP) in the LP30 electrolyte with current density 1 mA/cm² and various pulse lengths, T_{ON}, T_{OFF} . The linear fits are used to guide the eye.

6. SEM figures

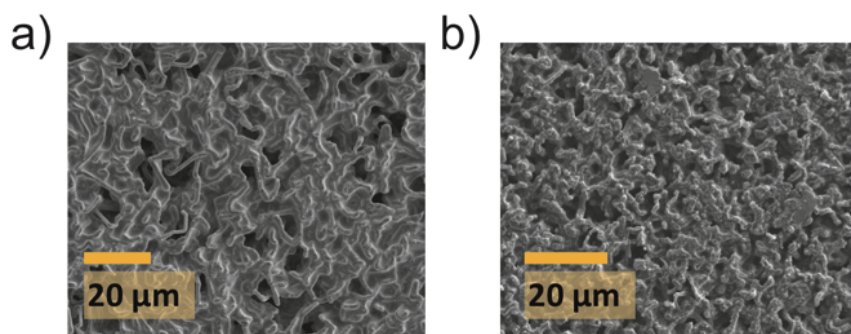


Figure S7. SEM of the microstructures formed during 2 mA/cm² constant current in a) LP30 and b) LP30 + 10% FEC

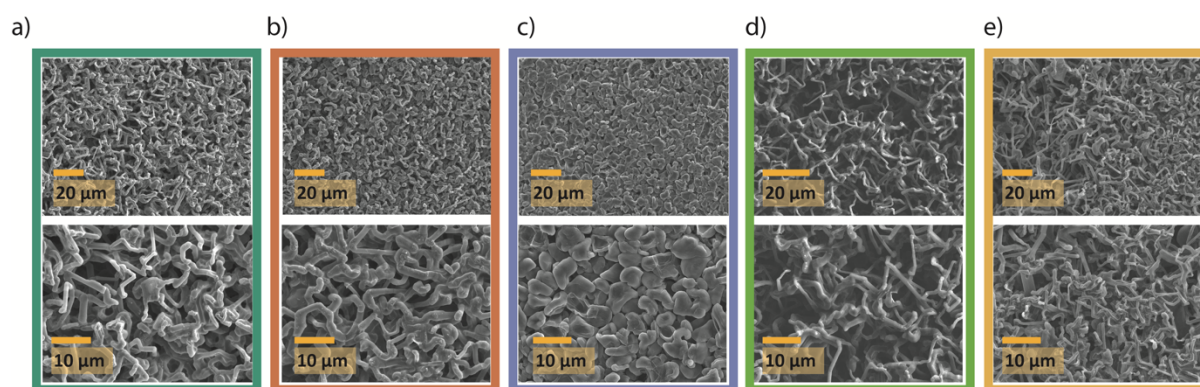


Figure S8. SEM images of the microstructures formed during a) constant plating with 0.5 mA/cm² and pulse plating with b) $T_{ON}, T_{OFF} = 1$ s c) $T_{ON}, T_{OFF} = 500$ ms d) $T_{ON}, T_{OFF} = 50$ ms and e) $T_{ON}, T_{OFF} = 5$ ms.

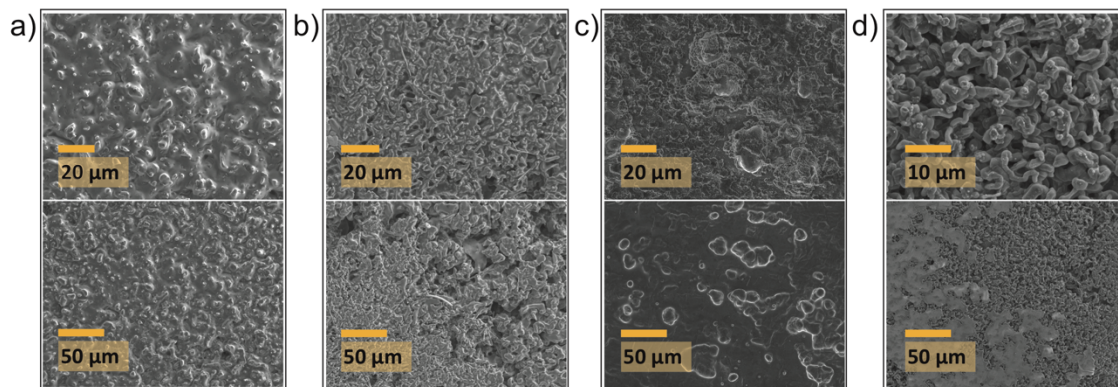


Figure S9. SEM images of the Li metal morphology during pulse plating with $T_{ON}:T_{OFF} = 5 \text{ ms}:15 \text{ ms}$ in **a)** LP30 and $j_{\text{instantaneous}} = 1 \text{ mA/cm}^2$ **b)** LP30 and $j_{\text{instantaneous}} = 2 \text{ mA/cm}^2$ **c)** LP30 + 10% FEC and $j_{\text{instantaneous}} = 1 \text{ mA/cm}^2$ **d)** LP30 + 10% FEC and $j_{\text{instantaneous}} = 2 \text{ mA/cm}^2$. The top row shows an image at high magnification while the bottom row shows an image at a lower magnification for each individual sample.

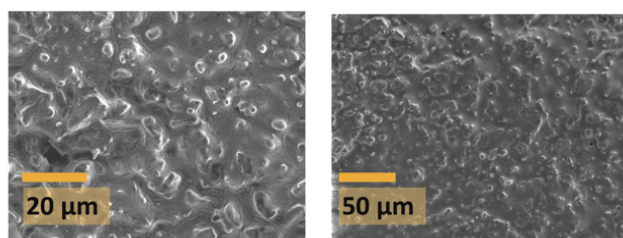


Figure S10. SEM images of the Li metal morphology during pulse plating in LP30 with $T_{ON}:T_{OFF} = 5 \text{ ms}:15 \text{ ms}$, like in Figure S24a above, after rinsing with anhydrous DMC.

7. The effect of pitting on the NMR measurements

To look at the effect of pitting on the stripping electrode, the *in situ* cell for pulse plating at 2 mA/cm^2 with $T_{\text{ON}}:T_{\text{OFF}} = 5\text{ms}:15\text{ms}$, was disassembled after cycling and NMR spectra taken of both the counter and working electrode separately, *ex situ*.

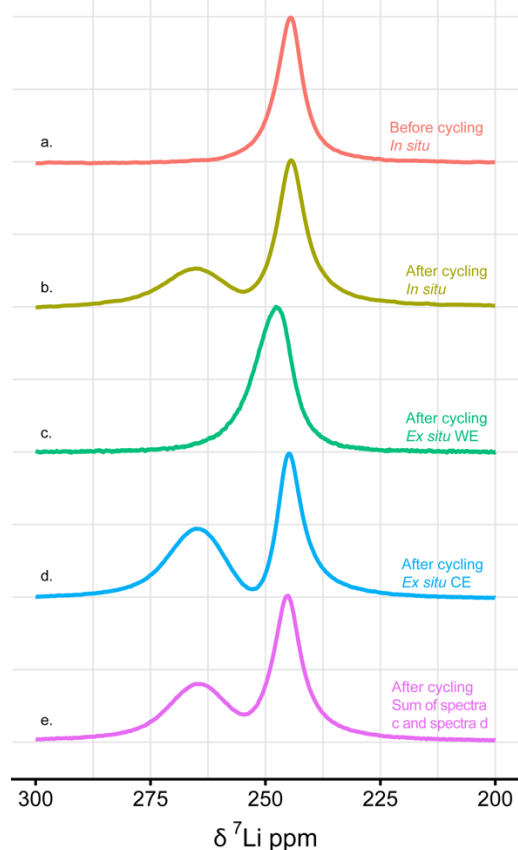


Figure S11. *Ex situ* NMR spectra of pitting on the stripping electrode Static ^7Li NMR spectra **a)** the symmetrical Li-Li cell, *in situ*, before cycling, **b)** the symmetrical Li-Li cell, *in situ*, after cycling, **c)** *ex situ* NMR of the disassembled cell on the plated electrode (working electrode, WE), **d)** *ex situ* NMR of the disassembled cell on the stripping electrode (counter electrode, CE), and **e)** the sum of spectra c and d, of the WE and CE. The metal peak of the stripping electrode after cycling, shown in green, has shifted to higher frequency (247.5 ppm compared to 245 ppm before cycling) and indicates roughening of the electrode surface.⁸

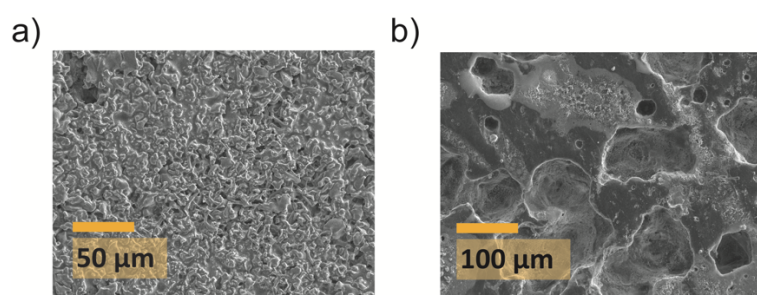


Figure S12. Pitting of the stripping electrode SEM images of the Li metal counter electrode (left) also shown in the main text, Figure 6f, and the working electrode (right). The pits that form on the working electrode are seen clearly.

8. Isotope exchange measurements

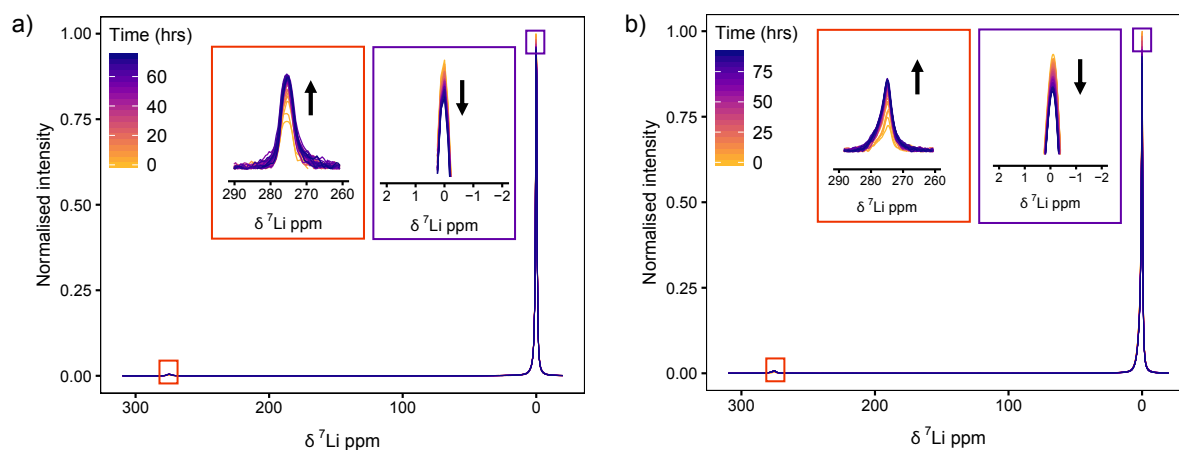


Figure S13. The NMR spectra of the isotope exchange measurements ${}^7\text{Li}$ NMR spectra of the electrolyte (around 0 ppm) and metal (around 275 ppm) during the 75 hour time period that the ${}^6\text{Li}$ -enriched strip of metal was soaked in natural abundance **a)** LP30 electrolyte (also shown in the main text, Figure 8a) and **b)** LP30 + 10% FEC electrolyte.

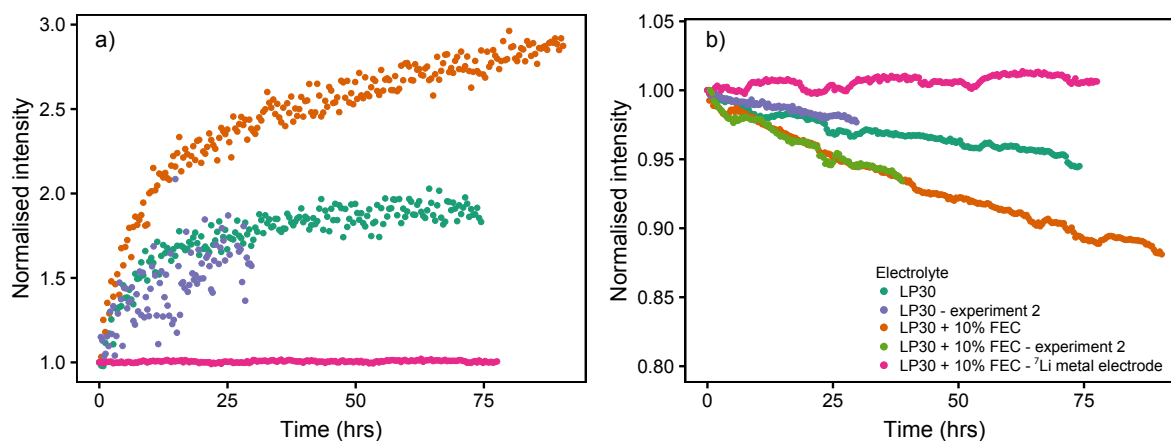


Figure S14. Reproducibility of the isotope exchange measurements. The intensity changes of the ${}^7\text{Li}$ NMR spectra recorded over 75 hours for **a)** the lithium metal signal and **b)** the lithium ions the two electrolytes LP30 (green) and LP30 + 10% FEC (orange) with both shorter experiments for both electrolytes included (purple and light-green) and an experiment using natural abundance ${}^7\text{Li}$ metal electrode in the soaking experiment (pink).

9. Numerical model of isotope exchange – Additional figures

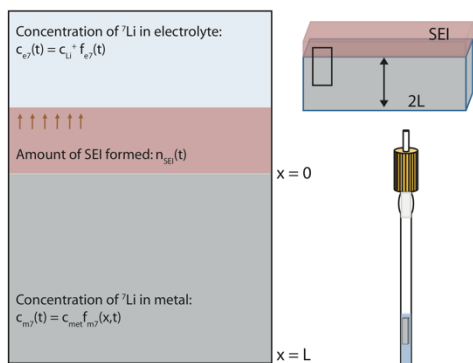


Figure S15. A schematic showing the geometry of the model and the experimental setup of a Li metal, soaked in an electrolyte in a sealed J-Young NMR tube.

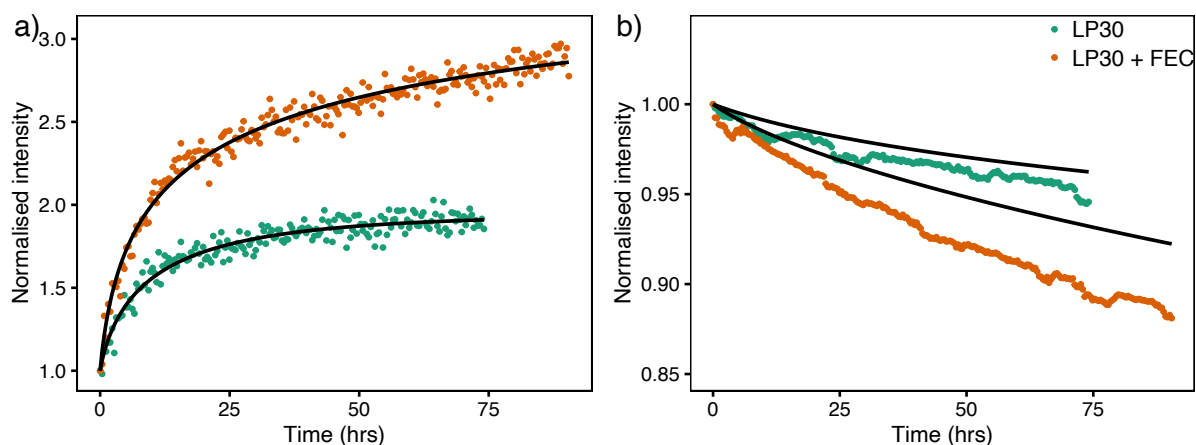


Figure S16. The resulting fit (filled lines) when equation 7 is used to describe the evolution of the ^7Li in the electrolyte c_{e7} , not taking into account how the SEI formation affects the isotope ratio as is done in equation 13; that is using equations 1-3 and 5-12 for **a)** the lithium metal signal and **b)** the lithium ions in the two electrolytes LP30 (green) and LP30 + FEC (orange). The fit underestimates the decrease in the diamagnetic ^7Li intensity during the NMR experiment and demonstrates how the SEI formation affects the $^{6,7}\text{Li}$ ratio and equation 7 needs to be modified to equation 13.

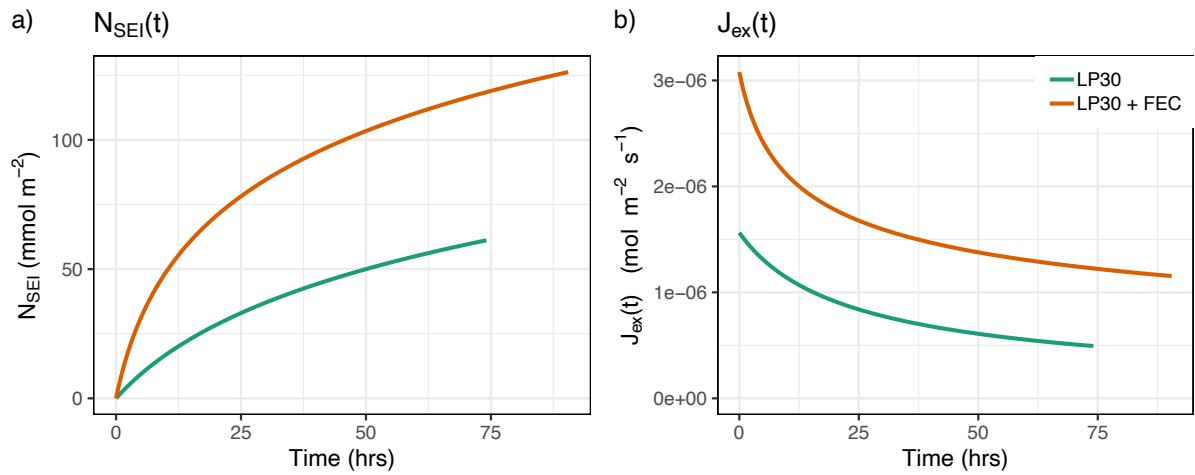


Figure S17. a) Number of moles of SEI formed per surface area of Li metal during the simulation of the isotope exchange and **b)** the evolution of the exchange rate constant $J_{ex}(t)$ with the growing SEI in the two electrolytes LP30 (green) and LP30 + FEC (orange).

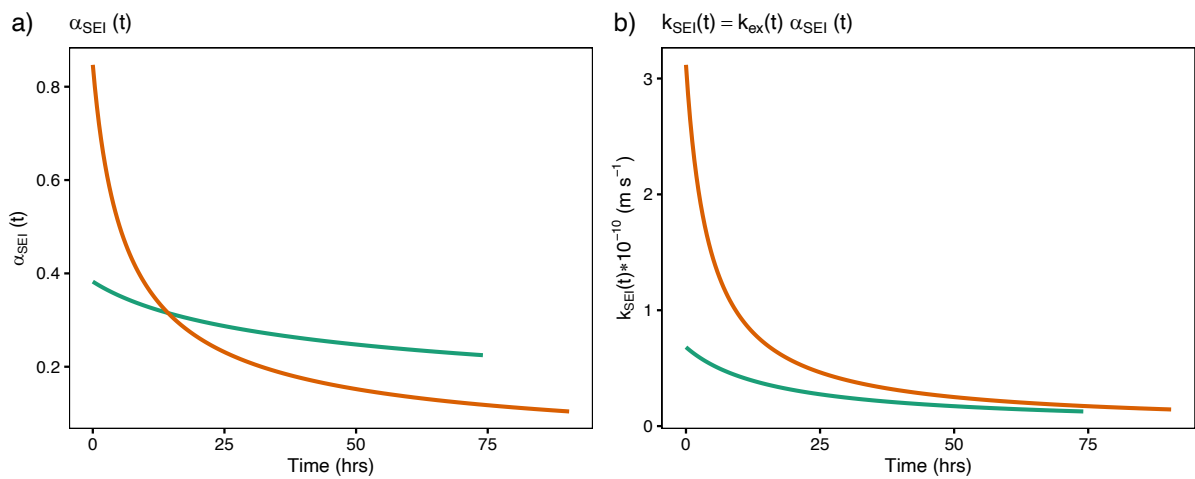


Figure S18. a) The evolution of the parameter $\alpha_{SEI}(t) = \alpha_{SEI,0} \exp(-\beta_{SEI} N_{SEI}(t))$ **b)** The evolution of the SEI formation rate constant $k_{SEI}(t) = \alpha_{SEI}(t)k_{ex}(t)$ with the growing SEI in the two electrolytes LP30 (green) and LP30 + FEC (orange).

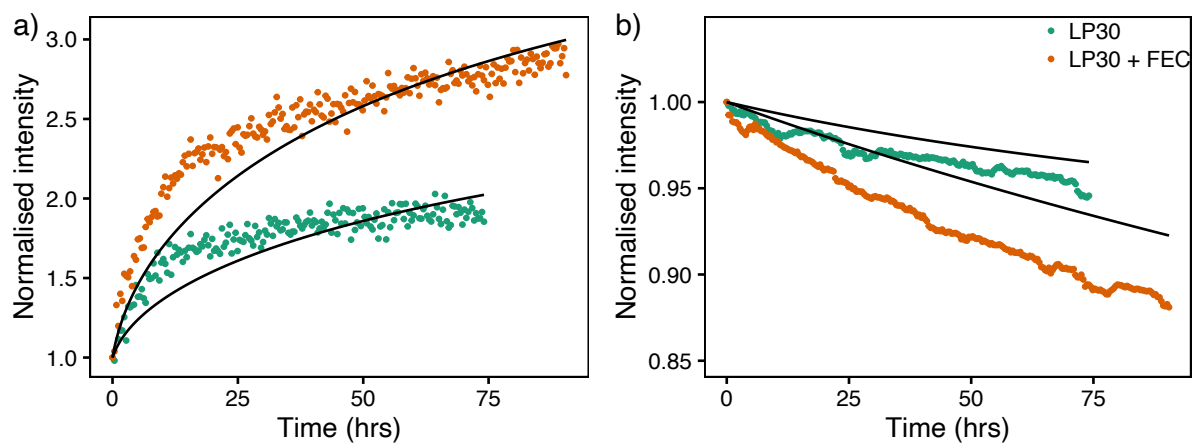


Figure S19. Sensitivity analysis using fixed values of $J_{ex,0}$ The fit obtained when using Model II with $J_{ex,0}$ fixed to the values obtained for J_{ex} in Model I, i.e. 0.77×10^{-6} mol m⁻² s⁻¹ for LP30 and 1.5×10^{-6} mol m⁻² s⁻¹ for LP30 + FEC, see discussion in main text.

Table S3. The 95% confidence intervals of the fitted model parameters for the isotopic exchange in the electrolytes, LP30 and LP30 + FEC, Model II.

Symbol	Description/Unit	LP30	LP30 + FEC
$J_{ex,0}$	Isotope exchange flux [10^{-6} mol m^{-2} s^{-1}]	1.5-1.7	2.9- 3.3
β_{ex}	SEI permeability constant [m^2 mol^{-1}]	6.8 - 31	5.3 – 10
$\alpha_{SEI,0}$	SEI formation proportionality constant Dimensionless	0.13 - 0.63	0.53 – 1.2
β_{SEI}	SEI growth constant [m^2 mol^{-1}]	0 - 18	11 – 23

10. Impedance spectroscopy

Potentiostatic electrochemical impedance spectroscopy (PEIS) was performed at open circuit voltage (OCV) and used to monitor the SEI impedance growth in symmetrical Li coin cells. The Nyquist plots of for both electrolytes can be seen in Figure S22. The impedance data was fitted to the equivalent circuit displayed in Figure S23, using a home-built MATLAB code and a non-linear least square solver, lsqcurvefit. The resistances of the compact SEI layer (R_1), the porous SEI layer (R_2) and the charge transfer resistance (R_3) were combined into $R_{SEI} = (R_1 + R_2 + R_3)/2$, divided by two to account for the two Li metal electrodes. R_{SEI} is shown as a function of time in Figure S24, where the impedance increases steadily over time in the LP30 electrolyte, whereas it stabilises in the LP30 + FEC electrolyte.

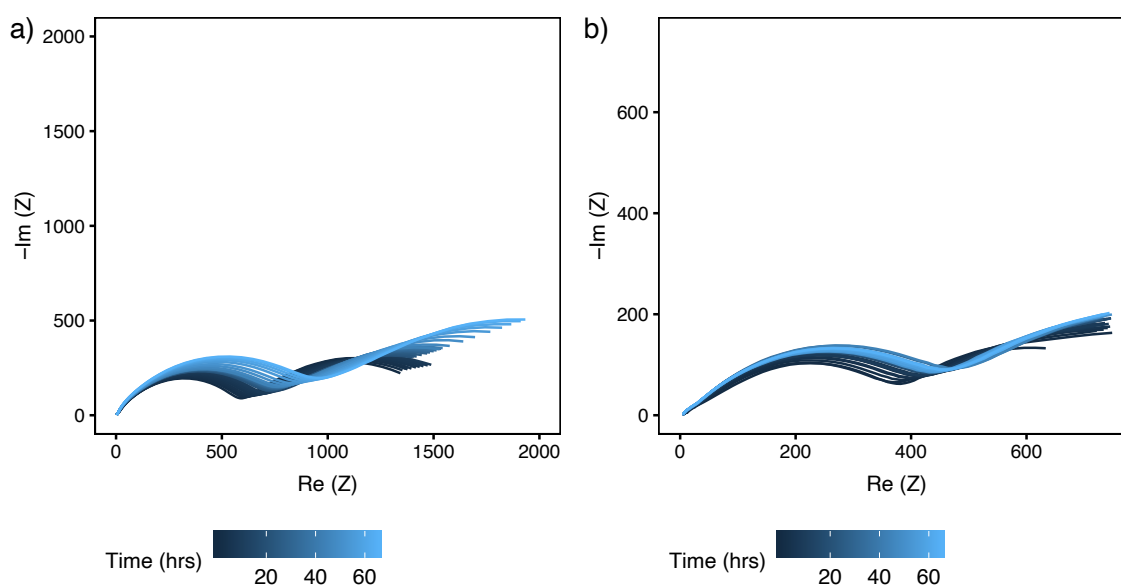


Figure S20. The Nyquist plot for symmetric Li-Li coin cells at OCV in **a)** LP30 electrolyte and **b)** LP30 + FEC.

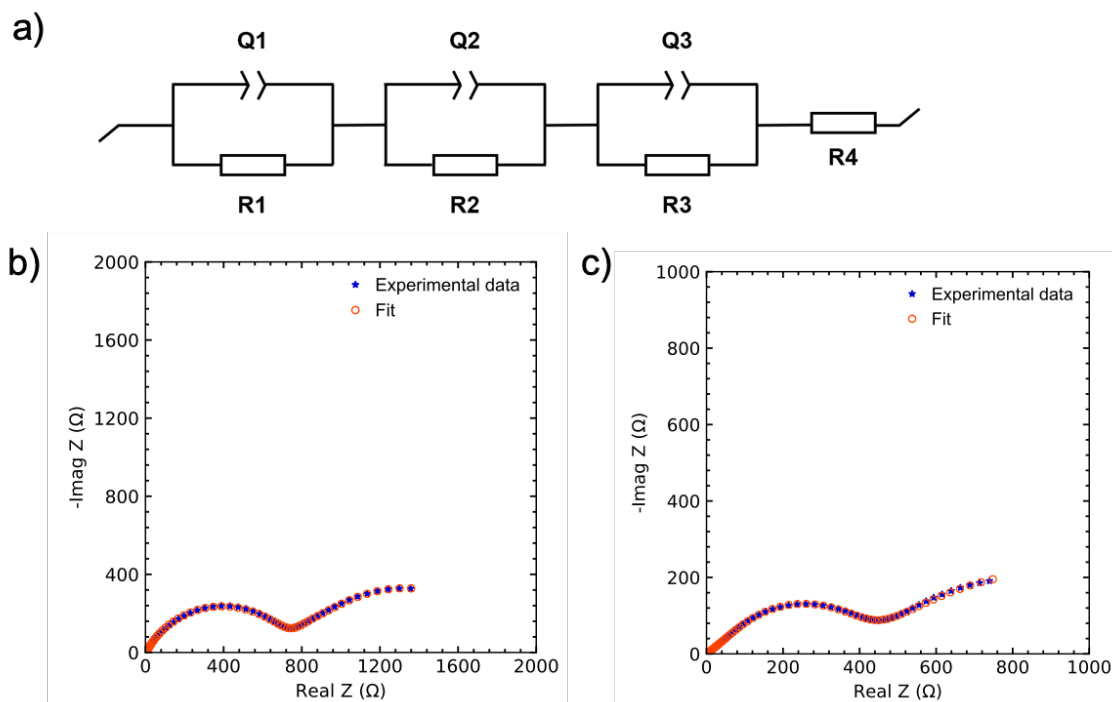


Figure S21. The equivalent circuit model and the corresponding fit a) The equivalent circuit used to fit the spectra, where R_1 and Q_1 (C_1 , capacitance and a_1 , parameter which describes how close it is to an ideal capacitor) are the resistance and the constant phase element (CPE) for the SEI compact layer respectively, R_2 and Q_2 (C_2 and a_2) are the resistance and the CPE element of the porous part of the SEI layer respectively, R_3 and Q_3 (C_3 and a_3) are the resistance and the CPE element for the charge transfer between SEI film and electrolyte, and R_4 is the bulk electrolyte resistance. The model was taken from a previous study on the formation of surface films on Li metal in different electrolytes.⁹⁻¹¹ b) The fit to the EIS data in LP30, at time = 12 hrs. c) The fit to the EIS data in LP30 + FEC, at time = 12 hrs.

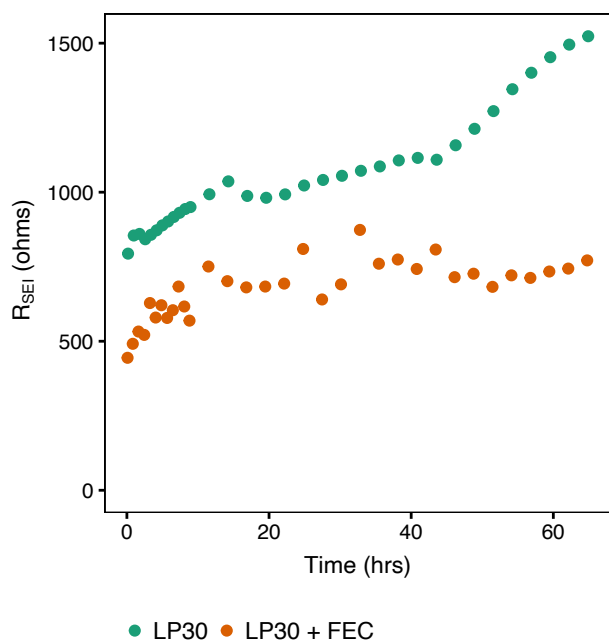


Figure S22. The resistance of the SEI on Li metal, $R_{SEI} = (R_1 + R_2 + R_3)/2$, determined from the fitting of the impedance spectra in LP30 (green) and LP30 + FEC (orange). The resistance of the LP30 + FEC is both lower and reaches an equilibrium value whereas for LP30 it continues to increase with time.

11. *In situ* NMR spectra and the electrochemistry

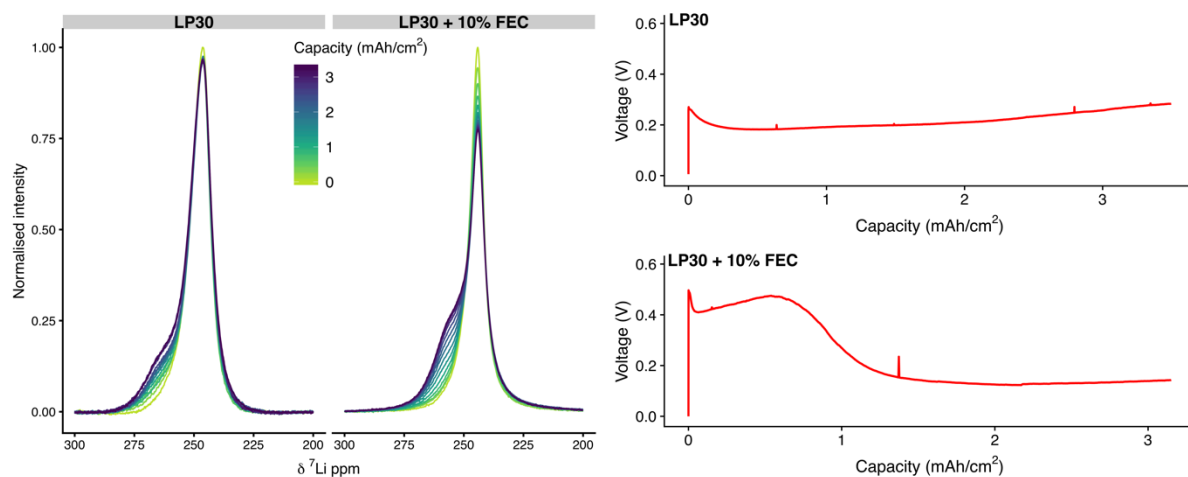


Figure S23. *In situ* NMR spectra obtained under a constant current of 0.5 mA/cm² in LP30 and LP30 + FEC. Deconvolution of the peaks is shown in Figure 2 in the main text.

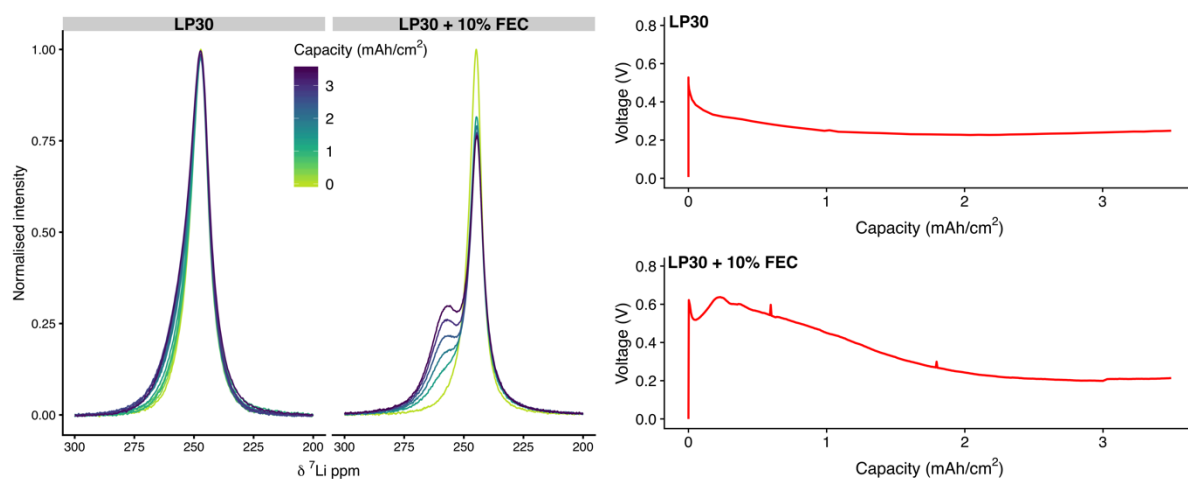


Figure S24. *In situ* NMR spectra obtained under a constant current of 1 mA/cm² in LP30 and LP30 + FEC. Deconvolution of the peaks is shown in Figure 3 in the main text.

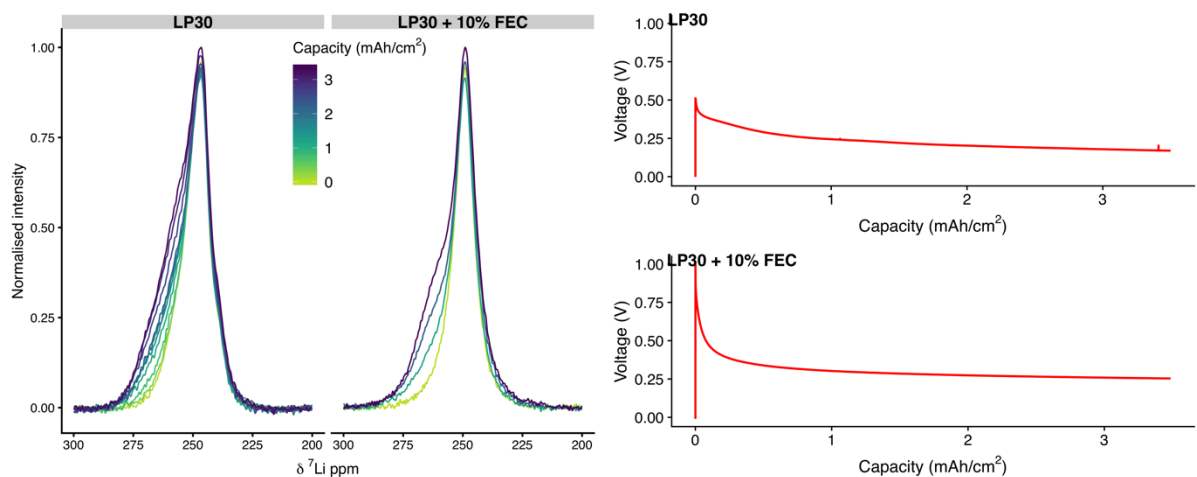


Figure S25. *In situ* NMR spectra obtained under a constant current of 2 mA/cm² in LP30 and LP30 + FEC. Deconvolution of the peaks is shown in Figure 3 in the main text.

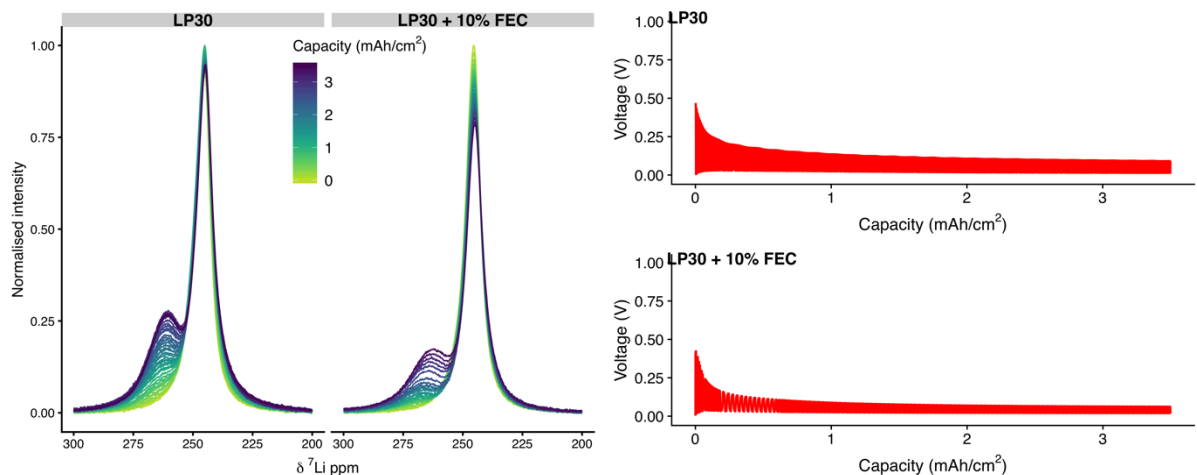


Figure S26. *In situ* NMR spectra obtained under a pulsed current of 1 mA/cm² for $T_{ON} = 1$ s and $T_{OFF} = 1$ s, in LP30 and LP30 + FEC. Deconvolution of the peaks is shown in Figure 6a for LP30 and Figure 7a for LP30 + FEC in the main text.

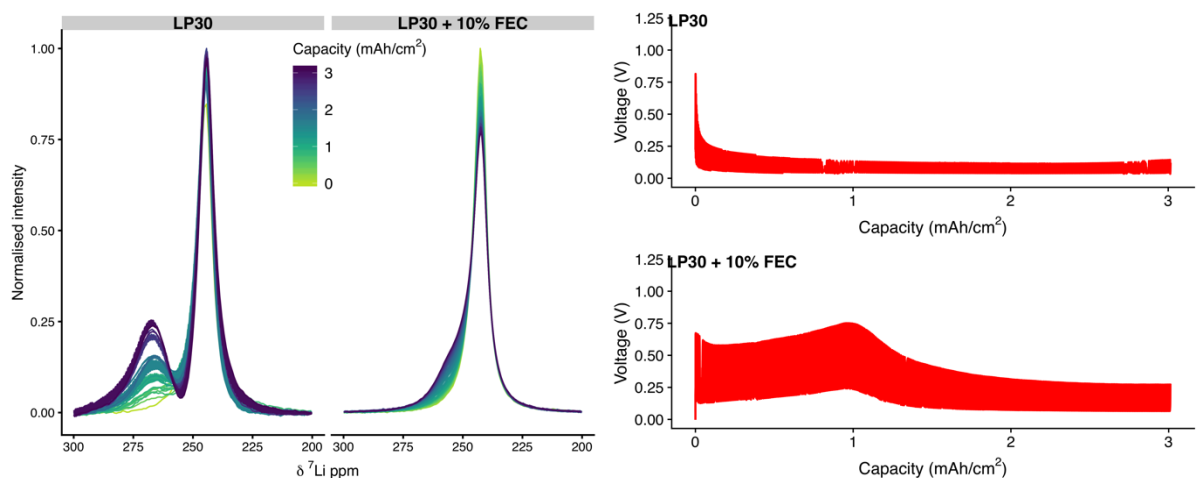


Figure S27. *In situ* NMR spectra obtained under a pulsed current of 1 mA/cm² for $T_{ON} = 5$ ms and $T_{OFF} = 5$ ms, in LP30 and LP30 + FEC. Deconvolution of the peaks is shown in Figure 6a for LP30 and Figure 7a for LP30 + FEC in the main text.

References

- 1 R. Bhattacharyya, B. Key, H. Chen, A. S. Best, A. F. Hollenkamp and C. P. Grey, *Nat. Mater.*, 2010, **9**, 504–510.
- 2 S. Chandrashekar, N. M. Trease, H. J. Chang, L.-S. S. Du, C. P. Grey and A. Jerschow, *Nat. Mater.*, 2012, **11**, 311–315.
- 3 C. Kittel, *Wiley Sons, New York, NY*.
- 4 D. R. Lide, *Handb. Chem. Phys.*, , DOI:10.1136/oem.53.7.504.
- 5 A. J. Ilott, S. Chandrashekar, A. Klöckner, H. J. Chang, N. M. Trease, C. P. Grey, L. Greengard and A. Jerschow, *J. Magn. Reson.*, 2014, **245**, 143–149.
- 6 D. I. Hoult, *Concepts Magn. Reson.*, 2000, **12**, 173–187.
- 7 H. J. Chang, N. M. Trease, A. J. Ilott, D. Zeng, L. S. Du, A. Jerschow and C. P. Grey, *J. Phys. Chem. C*, 2015, **119**, 16443–16451.
- 8 L. E. Marbella, S. Zekoll, J. Kasemchainan, S. P. Emge, P. G. Bruce and C. P. Grey, *Chem. Mater.*, 2019, **31**, 2762–2769.
- 9 D. Aurbach and A. Zaban, *J. Electrochem. Soc.*, 1994, **141**, 1808–1819.
- 10 A. Zaban, E. Zinigrad and D. Aurbach, *J. Phys. Chem.*, 1996, **100**, 3089–3101.
- 11 D. Aurbach and A. Zaban, *J. Electroanal. Chem.*, 1994, **365**, 41–45.